Control of Pneumatic Muscle Actuators

Darwin G. Caldwell, Gustavo A. Medrano-Cerda, and Mike Goodwin

Problems with the control and compliance of pneumatic systems have prevented their widespread use in advanced robotics. However, their compactness, power/weight ratio, and simplicity are factors that could potentially be exploited in sophisticated dextrous manipulator designs. This paper considers the development of a new high power/weight and power/volume braided pneumatic muscle actuator (PMA) having considerable power output potential, combined with controllable motion and inherent compliance to prevent damage to handled objects. Control of these muscles is explored via adaptive pole-placement controllers. Experimental results indicate that accurate position control of 1° is feasible, with power/weight outputs in excess of 1kW/kg at 200kPa.

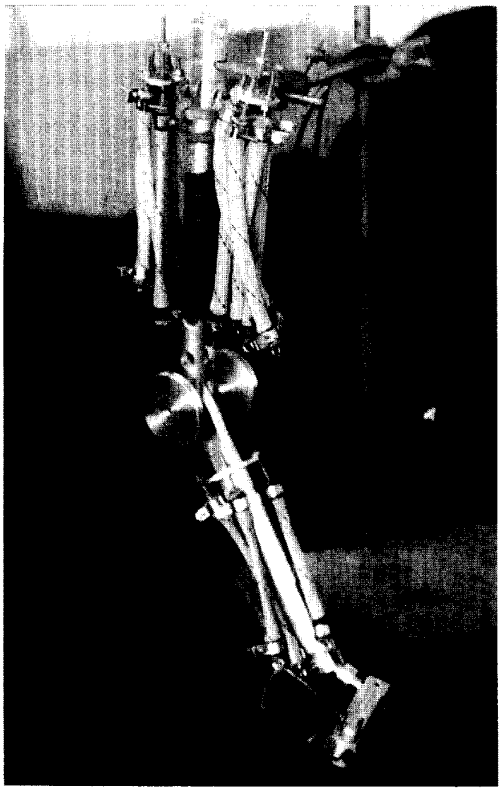

Actuators and actuation systems are essential features of all robots, providing the forces, torques, and mechanical motions needed to move the joints, limbs, or body. Their performance is characterized by parameters such as power (in particular the power/weight and power/volume ratios), strength, response rate, physical size, speed of motion, reliability, controllability, compliance, and cost.

Industrial robots have used three primary power sources: electric motors (primarily DC and AC), hydraulic cylinders, and pneumatic cylinders. Each of these actuation systems has well-documented advantages and disadvantages (Table 1), which, in spite of their widespread use, have hampered the development of advanced, truly flexible, compact robotic systems [1-2].

The limitations of these various prime movers have prompted research into a number of new technologies, such as piezoelectric actuators for controlled micro-manipulation and use in micro-robotics [3], shape memory alloy actuators with very high power/weight outputs [4-5], electro-rheological fluids for enhanced hydraulic operations [6-7], polymeric artificial muscle actuators which attempt to replicate the natural chemo-mechanical cycle [8-11], and magnetostrictive materials with high force generation potential when energized in a strong magnetic field [12]. Most of these developments have tended to draw on electric and hydraulic techniques, but there is also potential for the development of the most simple of the prime movers: pneumatics.

Pneumatics cylinders have been used for many years and are well adapted to simple repetitive tasks requiring only a very limited amount of system control. They have not, however, been widely applied in advanced robotics due primarily to two interrelated problems: (1) the accuracy and difficulty of control and (2) compliance (sponginess), which means that load variations have a significant effect on position [13]. Both these problems are due to the compressibility of the fluid (air), and although partial solutions have been found by carefully controlling the venting of the cylinders, the problems largely remain [14].

This work considers the development and control of a new braided pneumatic actuation system (pneumatic muscle actuators) for use in high power/weight, power/volume robotic appli-

Table 1. Comparison of actuators.

Actuator	Advantages	Disadvantages
Pneumatics	Cheap, quick reponse time, simple "bang-bang" control.	Position control difficult, fluid compressible, noisy.
Hydraulics	High power/weight ratio, low backlash, very strong, direct drive possible.	Less reliable, expensive, servo control complex, noisy.
Electrics	Accurate position and velocity control, quiet, relatively cheap.	Low power and torque/weight ratios, possible sparking.

The authors are with the Department of Electronic Engineering, University of Salford, Manchester M5 4WT, U.K.

0272-1708/95/$04.00©1995IEEE

cations. The relationships between interweave angle and actuator surface area, volume, and forces generated are established. The inherent non-linearities of these actuators are a major obstacle for designing conventional control systems which yield a reasonable performance over a wide range of operating conditions. The performance of pneumatic systems can, however, be considerably improved by using adaptive controllers. The adaptive scheme considered in this paper is based on explicit on-line estimation of a parametric model for the overall system (valve, muscle, sensor, and anti-aliasing filter). The estimated model is used to determine a basic controller using a pole-placement method. This basic controller is then suitably enhanced to improve stability margins and performance of the closed-loop system. Experimental results for a powered robotic elbow driven by five parallel connected pneumatic muscles are presented.

Pneumatic Actuators

Pneumatic cylinders have formed a simple low-cost actuation source which has been used for many years in mechanical and prosthetic applications, but problems with the control and compliance of pneumatic systems have prevented their widespread use in advanced robotics [15]. Their compactness, power/weight ratio, and inherent safety are, however, factors that could potentially be exploited in sophisticated dextrous manipulator designs.

The cylindrical nature of the these actuators and the fact that the drive force is transmitted to a piston using air, which is a compliant agent, means that loading and variations in the pressure of the supply and other mechanical parameters cause considerable changes in the positional accuracy of the system.

To overcome these shortcomings, a number of newer pneumatic systems have been developed, generally based on the use of rubber or some similar elastic material [15-21]. This forms a seal to limit and control the expansions of the air and hence control the overall motion of the actuator. Many of these actuators were developed in the 1950s and 1960s for use in prosthetic applications, but the use of electrically powered prosthesis controlled by myoelectric signals has led to their replacement. The major drawbacks at that particular time were the need for a compressed air supply and the simpler control aspects of electric motors.

Although the use of electric motors meant that pneumatic techniques were largely discontinued in prosthetics, there was continued work on specialized actuators for use in high power/weight robotic projects, many of these being for very sophisticated dextrous manipulator applications. These systems typically used double acting actuators for direct drive [22-23].

There has also been renewed interest in variants of a system developed in the 1950s and 1960s for prosthetic/orthotic applications, the McKibben Muscle [15]. Systems that use this form of technology include the ROMAC [16], Rubbertuator [17], Flexator [18], and braided pneumatic muscle actuators (PMA) [19-21] studied here.

Actuator Design

The pneumatic muscle actuator (PMA) is constructed as a two-layered cylinder (see Fig. 1). The inner layer is made from thin-walled rubber tubing, with two perspex plastic plugs (one with an air inlet/exhaust pipe) forming the termination connectors to seal the ends of the tube. This acts as a pressurized containment unit. Around the rubber tubing there is a flexible

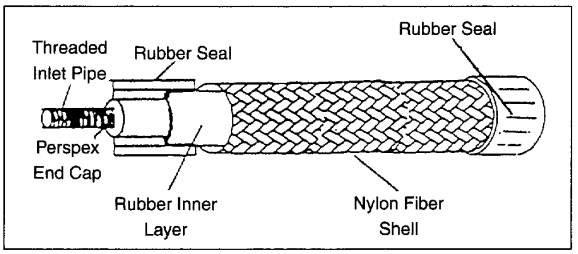

Fig. 1. Pneumatic muscle actuator design.

sheathing formed from high-strength interwoven (but not bonded) nylon fibers. The flexibility of this structure means that it can be stretched or compressed without damage, while the shell prevents the delicate rubber liner from over-inflating and rupturing [19, 24]. Both the liner and the nylon shell are bonded to the end-caps using a flexible adhesive and clamped securely in place using a rubber sealing ring. The complete unit can safely withstand pressures up to 750kPA (7.5 bar), although 200-300kPa is a more usual operating pressure.

In its natural unstrained condition a typical actuator is 79mm long, with a diameter of 12.7mm, an interweave angle (angle of fiber cross-over) of 59.3° and a mass of 10.5g. These dimensions, together with data on the actuator when fully compressed and expanded, are recorded in Table 2.

Table 2. Actuator stressed and compressed data.

	Length	Diameter	Interweave Angle
Compressed	52mm	14.2mm	70.0°
Unstrained	79mm	12.7mm	59.3°
Elongated	143mm	4.8mm	20.0°

System Model Performance

To function as an actuator, the pneumatic muscle must be capable of generating some form of usable drive force, and to determine the potential of the system a performance model has been produced.

The factors critical in the determination of the driving force in any pneumatic system are the pressure difference and the area over which a distortion pressure is applied. With conventional cylinders, only the piston face plate is free to move, and only this area is critical. In the braided muscle, the flexibility of the structure means the whole shell/liner interface provides a significantly larger drive area.

The braided structure of the external nylon shell means that the muscle may be considered as a series of two-dimensional trapezoids. These trapezoids are pressurized by the inner shell, and this forms the drive plate comparable to the piston area in the cylinder. In this design, as the actuator stretches or compresses the interweave angle will change, and indeed the whole surface area of the muscle varies. To determine the driving force it is therefore essential that the surface area at any interweave angle or length be known.

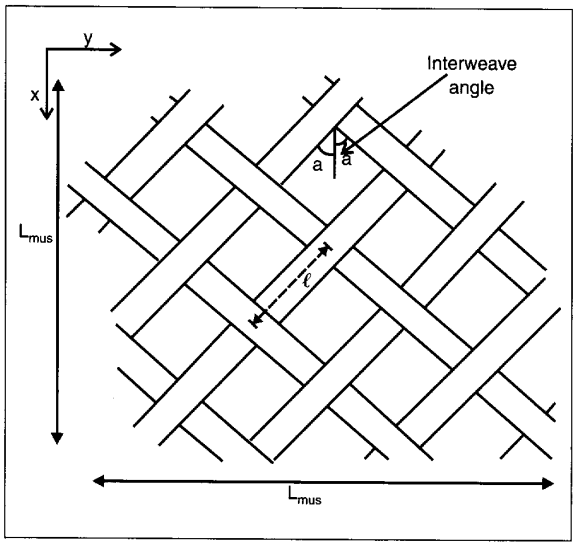

Fig. 2. Interweave angle.

If the cylindrical muscle is "opened" (Fig. 2), the two-dimensional nature is easily observed. If l is the length of one side of the trapezoid, the overall length of the muscle is:

$$L_{mus} = 2*A*l \cos a_{mus} = h \cos a_{mus} \quad (1)$$

where A is the number of trapezoids in the x plane, h is helical fiber length (h= 2Al), and a_{mus} is the interweave angle. Similarly, in the y direction the circumference is:

$$C_{mus} = 2*B*l \sin a_{mus} \quad (2)$$

where B is the number of trapezoids in the y plane (around the muscle body). Since the circumference is proportional to the diameter this becomes:

$$D_{mus} = f \sin a_{mus} \quad (3)$$

where f is the diametric distance parameter and equals $2Bl/\pi$.

Using the compressed and elongated data in Table 2, these equations may be solved.

$$h = (L_{max})/\cos a_{max} = (L_{min})/\cos a_{min} \quad (4)$$

$$= 143/\cos 20.0 = 52/\cos 70.0 = 152\text{mm}$$

$$f = (D_{max})/\sin a_{max} = (D_{min})/\sin a_{min} \quad (5)$$

$$= 14.2/\sin 70.0 = 4.8/\sin 20.0 = 14.5\text{mm}$$

The values for h and f are averaged from the compressed and elongated data to reduce measurement error.

Having computed h and f, which will be constant for all actuators of equal dimensions, the surface area, S_a, at any interweave angle can be determined;

$$S_a = \pi * D_{mus} * L_{mus} = \pi * (f \sin a_{mus}) * (h \cos a_{mus}) \quad (6)$$

As would be expected, the maximum surface area is obtained when the interweave angle is 45°, giving a crossover angle of 90°. Fig. 3 shows the normalized surface area/interweave angle relationship.

The second parameter involved in the determination of any pneumatic force output is the pressure. In this instance it is necessary to study the changes in internal pressure as the muscle expands and contracts, which is again linked to the interweave

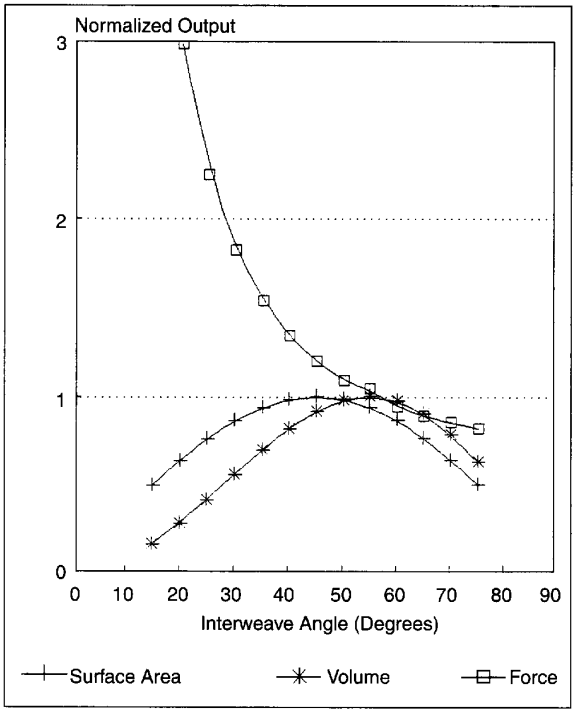

Fig. 3. Normalized relationships.

angle. From the basic Gas Laws, pressure is known to be inversely proportional to volume. The volume of the actuator cylinder is computed using (1) and (3), the actuator length at any interweave angle L_{mus}, and the corresponding diameter D_{mus}:

$$Vol = (D_{mus}2/4) * \pi * L_{mus} = K (\sin a_{mus})^2 (\cos a_{mus}) \quad (7)$$

where $K = (\pi/4)*f^2*h$. Fig. 3 shows the normalized volume/interweave angle relationship, with maximum volume, and therefore the minimum pressure occurring at an interweave angle of 54.5°. At this minimum internal pressure the actuator is in its most stable condition.

Any changes from this state (either from elongation or compression) will cause an increase in pressure and induce a force to return to the minimum energy state. It is this return force that can be used to drive the actuator. If the muscle is elongated, contraction results in a pressure reduction, while in a compressed state the muscle must extend to increase the volume and reduce the pressure.

The drive (restoring) force is produced as a result of the desire of the actuator to maintain its minimum energy/force state. In this minimum energy/force state the internal force is given by:

$$F_{min} = S_a P + 2E_a P = P(S_a + 2E_a) \quad (8)$$

where E_a is the area of the end plates, and P is the internal pressure.

When elongated or compressed from this point, the volume will reduce and a drive force will be produced. The force at any interweave angle is given by

$$F = S_a P_{new} + 2E_a P_{new} = P_{new}(S_a + 2E_a) \quad (9)$$

where P_{new} is the new internal pressure caused by a reduction in the system volume. The pressure change with interweave angle is the reciprocal of the volume change outlined above.

As the pneumatic actuators are a practical system, they are not 100% efficient, and the force output is typically only 40%-50% of the theoretically predicted values. Losses are attributed to line leakage, frictional effects, rubber elasticity, expansion energy for the liner, valve losses, and dead spaces. To take account of these effects, an efficiency conversion factor must be included. The actual practical driving force equation (modified from experimentation) is thus

$$F_d = E_{ff}(F - F_{min}) \quad (10)$$

E_{ff} is the force conversion factor. When the force is positive the actuator will contract, while a negative force will produce expansion.

Fig. 3 shows the normalized force output profile. At the maximum volume state (interweave angle = 54.5°) the internal force has been normalized to 1. Distortion from this "relaxed" condition will produce changes in the internal pressure which form the driving force. The output force ranges from 50N-75N at 200kPa (2 bar). The power output under these conditions is in the range 1-1.5kW/kg [19,24].

Arm Design

The arm which will be used for testing was designed with the initial specification that it should be used as a tele-operated unit driven from a data sleeve presently being developed. To this end it was essential that the layout of the manipulator should attempt to replicate the layout and dimensions of the human arm. For this purpose the arm was designed with a shoulder having three degrees of freedom, a wrist with three degrees of freedom (wrist rotation has been moved from an elbow-driven unit to the wrist for design simplicity) and a one-degree-of-freedom elbow. DC motors have been chosen to drive the three shoulder joints. The motors are located in the main body of the robot, and hence their masses do not affect the arm weight. In the elbow and the wrist the mass of the actuators presents a significant loading; thus PMAs have been chosen to drive these joints. In addition for duplication of the human input arm some compliance is not necessarily a drawback and could in fact be an asset. An initial design trial has been conducted using the elbow joint alone powered by a parallel network of muscle "cells" formed in a biceps.

The arm design is shown on page 40. The arm is designed to carry a load of 5kg. The required flexion of the elbow is through 120°. The arm has been constructed from aluminum and trimmed of excess material to reduce the loading.

Elbow Control

To demonstrate the effectiveness of the muscles and controller operation, 5 muscles were connected in parallel to the lower section of an elbow joint. The muscles in this application were designed to function as a biceps. Although care has been taken in the design and construction of the biceps unit, there were small variations in performance and size. This in effect replicates performance variations as found in human muscle and forms a test for the robustness of the controller.

Air flow and pressure regulation within this system are provided using electrically driven, low-power piezoelectric valves with a switching frequency of 40-50Hz (Hoerberger piezo 2000, 0.001W per valve). This relatively rapid response makes pulse width modulation under direct computer control feasible. To reduce transport delays and energy losses, the piping length from valves to muscles should be as short as possible. Stiction in the joints should be minimal; otherwise additional control problems may arise at low frequencies, for example when attempting to control elbow motion smoothly at low speeds. The amount of muscle contraction is to be controlled by varying the duty cycle of the pulse width modulator. The duty cycle is defined as a ratio of time intervals t_1/t_p, where t_p is the valve pulse period (25ms) and t_1 denotes the time interval when the muscle is connected to the pressurized air supply. The variable time t_1 can take values between zero and 25ms and hence the duty cycle is a dimensionless quantity taking values between zero and one.

Some typical relationships between the duty cycle and the position sensor readings are shown in Fig. 4. The two plots correspond to the same system, but one was taken after 10 minutes of continuous operation (warm muscle) while the other was taken at intervals from a "cold" start. The difference in these plots may be due to temperature variations caused by air flow friction along the rubber wall of the muscle. The system exhibits a non-linear and time-varying behavior (gravity effects are taken into account). Some hysteresis was also detected, and this may be due to the muscle characteristics and/or small amounts of joint stiction.

Adaptive Control System Design

In [19], discrete time PID controllers with a feedforward term were implemented for controlling a pneumatic muscle. This controller was tuned by trial and error to yield a suitable closed-loop bandwidth with little overshoot. Unfortunately, the closed-loop performance was quite sensitive to errors in the feedforward term, mainly due to supply pressure fluctuations, pipe length, temperature, and muscle characteristics. In [24], an alternative control scheme was investigated. The performance of this controller was significantly faster, but still dependent on the above factors. In this work we consider an adaptive controller based on the scheme in [24]. The corresponding block diagram is shown in Fig. 5. At each sampling interval the model polynomials $B(z^{-1})$, $A(z^{-1})$ are estimated. These parameters are then used to compute the controller polynomials $F(z^{-1})$, $G(z^{-1})$ and the constant H. The "integrator" has been incorporated in the forward path to guarantee zero steady state error for constant reference inputs.

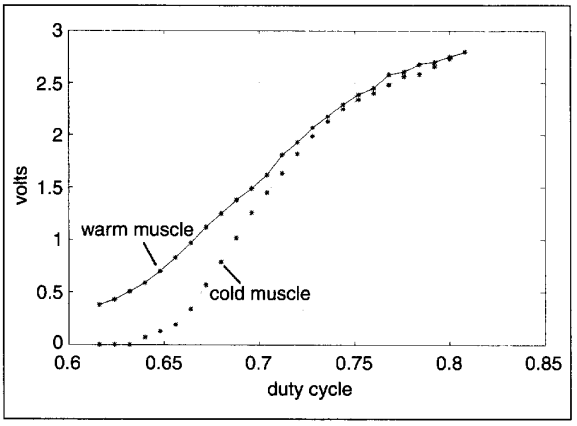

Fig. 4. Open-loop input-output steady-state relations at 200kPa (without loading).

Model Estimation

Experimental tests were carried out to obtain input-output data records. These records were used to estimate the parameters of a linear discrete model using off-line linear least squares methods. The inputs were generated by adding pseudo-random variations of a specified amplitude to a fixed duty cycle. The fixed duty cycle was chosen to correspond to the mid-point of the available range, Fig. 4.

The off-line analysis, using MATLAB, indicated that a model with 7 parameters and a time delay of 3 units (where one unit is a valve pulse period of 25ms) was adequate. The chosen model structure is given by

$$A(q^{-1})\, y(k) = B(q^{-1})\, u(k) + d + n(k) \qquad (11)$$

where $A(q^{-1}) = 1 + a_1 q^{-1} + a_2 q^{-2} + a_3 q^{-3}$, $B(q^{-1}) = b_0 q^{-3} + b_1 q^{-4} + b_2 q^{-5}$, and y, u, and n denote the position sensor reading, duty cycle, and unmeasurable noise, respectively. The constant d is used to model the effects of non-zero means in the input-output data. An average set of estimated values for the model {11} is given in Table 3. For on-line identification the model parameters are estimated using recursive least squares with a variable forgetting factor $\lambda(k)$:

$$\lambda(k) = \alpha * \lambda(k-1) + (1 - \alpha) * \beta(k)$$

$$\beta(k) = \begin{cases} \lambda_{min}, & \text{if estimation error (k)} \mid > \gamma \\ \lambda_{max}, & \text{if estimation error (k)} \mid <= \gamma \end{cases}$$

In our implementation we use a square root algorithm and the values $\alpha = 0.95$, $\Upsilon = 0.01$, $\lambda_{min} = 0.95$, $\lambda_{max} = 0.99999$.

Controller Design

From Fig. 5 the closed-loop transfer function is found to be

$$\frac{H\, B(z^{-1})}{(1 - z^{-1})\, A(z^{-1})\, F(z^{-1}) + B(z^{-1})\, G(z^{-1})} \qquad (12)$$

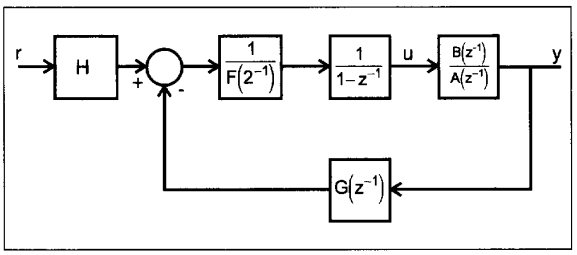

Fig. 5. Control system block diagram.

where the polynomials $F(z^{-1})$ and $G(z^{-1})$ are to be designed using a pole placement method, and H is computed to yield unity gain for constant inputs:

$$F(z^{-1}) = 1 + f_1 z^{-1} + f_2 z^{-2} + \ldots\ldots + f_{nf} z^{-nf} \qquad (13)$$

$$G(z^{-1}) = g_0 + g_1 z^{-1} + g_2 z^{-2} + \ldots\ldots + g_{ng} z^{-ng} \qquad (14)$$

$$H = G(1) = g_0 + g_1 + g_2 + \ldots. + g_{ng} \qquad (15)$$

Selecting the desired closed-loop characteristic polynomial to be

$$T_d(z^{-1}) = 1 - 2.64 z^{-1} + 2.3228 z^{-2} - 0.68112 z^{-3} \qquad (16)$$

(this yields an overdamped response with a time constant of 700ms), the pole-placement equation to be solved is

$$(1-z^{-1})\, A(z^{-1})\, F(z^{-1}) + B(z^{-1}) G(z^{-1}) = T_d(z^{-1}) \qquad (17)$$

Equation (17) has an infinite number of solutions which may be parameterized in terms of the minimum order polynomials $F_0(z^{-1})$ and $G_0(z^{-1})$ satisfying (17) ($F_0(z^{-1})$ and $G_0(z^{-1})$ are unique provided $B(z^{-1})$ and $(1-z^{-1})A(z^{-1})$ are relatively prime, i.e., have no common roots). The minimum order polynomials F_0 and G_0 are:

$$F_0(z^{-1}) = 1 + 0.8063 z^{-1} + 0.6525 z^{-2} + 0.4321 z^{-3} - 0.3403 z^{-4} \qquad (18)$$

$$G_0(z^{-1}) = 13.3012 - 34.5306 z^{-1} + 30.1477 z^{-2} - 8.8757 z^{-3} \qquad (19)$$

To enhance the relative stability of the closed-loop system the controller polynomials F and G are computed as follows:

$$F(z^{-1}) = F_0(z^{-1}) + B(z^{-1}) P(z^{-1}) \qquad (20)$$

$$G(z^{-1}) = G_0(z^{-1}) - (1-z^{-1})\, A(z^{-1}) P(z^{-1}) \qquad (21)$$

Table 3. Average estimated model parameters.

$a_1 = -2.4463$	$a_2 = 2.0028$	$a_3 = -0.5529$
$b_0 = 0.0078$	$b_1 = 0.0529$	$b_2 = -0.0212$
$d = -0.0237$		

where $P(z^{-1}) = p_0 + p_1z^{-1} + p_2z^{-2} + ... + p_{np}z^{-np}$ is computed such that the sum of the squares of the coefficients of $G(z^{-1})$ is minimized for a chosen value of np (note that $F(z^{-1})$ and $G(z^{-1})$ also satisfy (17)). In [25-27] it has been shown that this scheme tends to improve relative stability (and in some cases also closed-loop performance). For np=2 the controller polynomials are

$$F(z^{-1}) = 1 + 0.8063z^{-1} + 0.6525z^{-2} + 0.5229z^{-3} + 0.3253z^{-4} + 0.1086z^{-5} - 0.0286z^{-6} - 0.04335z^{-7} \quad (22)$$

$$G(z^{-1}) = 1.6653 - 0.847z^{-1} - 1.5356z^{-2} - 0.6826z^{-3} + 0.9102z^{-4} + 1.6601z^{-5} - 1.1279z^{-6} \quad (23)$$

For both controllers

$$H = 0.0425 \quad (24)$$

The preceding analysis indicates that both the minimum-order controller (18-19) (4th order) and the high-order controller (22-24) (7th order) satisfy the same pole assignment equation. The potential benefits of implementing the high-order controller can be revealed by frequency response plots of the loop gain $B(z^{-1})G(z^{-1})/(1-z^{-1})A(z^{-1})F(z^{-1})$. Figs. 7a and b show the Nyquist plots and the magnitude Bode diagrams of the loop gain for the model given in Table 3 and the controllers (18-19), and (22-24). The loop gain for the minimum order controller is unacceptably large in the frequency region 10-20Hz. Potentially the closed-loop system could become unstable when the model is not sufficiently accurate in this frequency region.

Experimental Results

At each sampling interval the sequence of the adaptive control algorithm is:

Step 1. Read position sensor and reference set-point.

Step 2. Compute duty cycle.

Step 3. Update model parameters.

Step 4. Compute controller parameters.

The model and controller parameters are initialized using the values in Table 3 and (22-24).

The scheme was implemented on a 486/50MHz personal computer in C. The overall program includes a general-purpose routine to carry out matrix manipulations, e.g., multiplication, addition, and inverse, and code to read and write experimental data to and from the hard disk (670 lines of code). The program is compiled to optimize execution speed but not memory requirements. The execution time for steps 1 and 2 is approximately 100 us, and 5ms for steps 3 and 4. The sampling time interval is 25ms, and the pulse width modulated signal is generated by timer interrupts.

All experimental data records were taken after 90 seconds at a supply pressure of 200kPa. Figs. 7 and 8 show the response for a square wave reference input. A significant improvement in performance is achieved using the high-order controller. Fig. 9 compares the experimental response with simulation results using the (fixed) parameter values given in Table 3 and controller (22-24). Fig. 10 shows the response for a smoothed square wave reference input.

Fig. 11 illustrates changes in the output when the supply pressure is increased from 200kPa to 300kPa, while Fig. 12 shows the effects of adding and removing a 0.325kg load. These figures illustrate that the closed-loop performance is reasonably robust with respect to pressure and load variations. Fig. 13 shows the steady state response for sinusoidal reference waveforms.

Conclusions

For future generations of robots, especially those required to work autonomously or semi-autonomously in non-factory environments, there are many key sectors that require development, but among the most vital is the actuation system.

Pneumatic actuation systems have well-documented advantages and disadvantages; however, the drawbacks of poor control and sponginess have been vital in limiting their use in advanced robotics.

Braided pneumatic muscle actuators, which have a structure totally alien to conventional cylinders, have all the traditional benefits of safety, relative simplicity, and inherent compliance regulation combined with very superior power/weight ratios (in excess of 1kW/kg at 200kPa) and compactness.

These performance characteristics have potential in all areas of system actuation, but particular benefits may be in manipula-

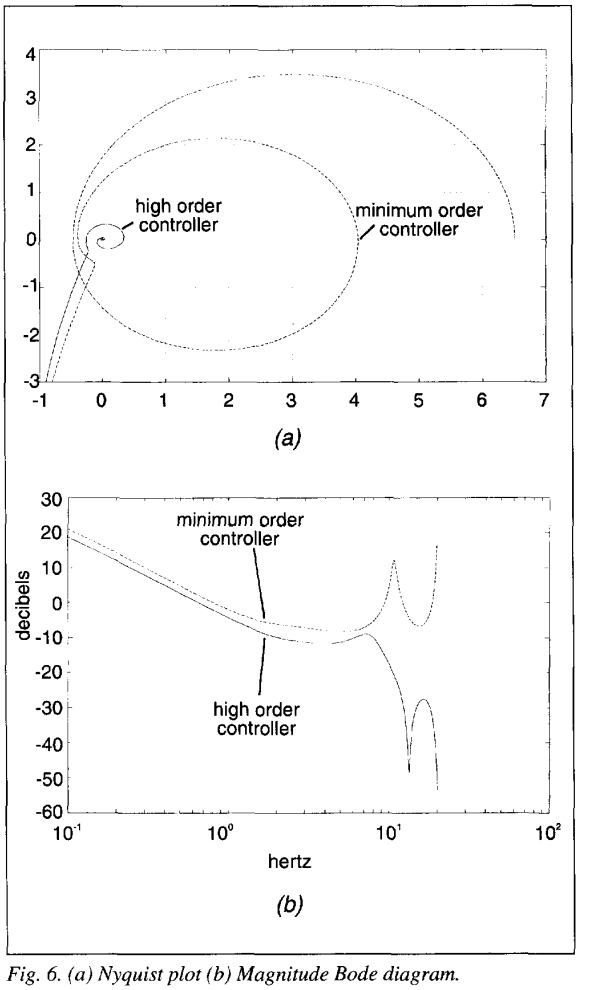

Fig. 6. (a) Nyquist plot (b) Magnitude Bode diagram.

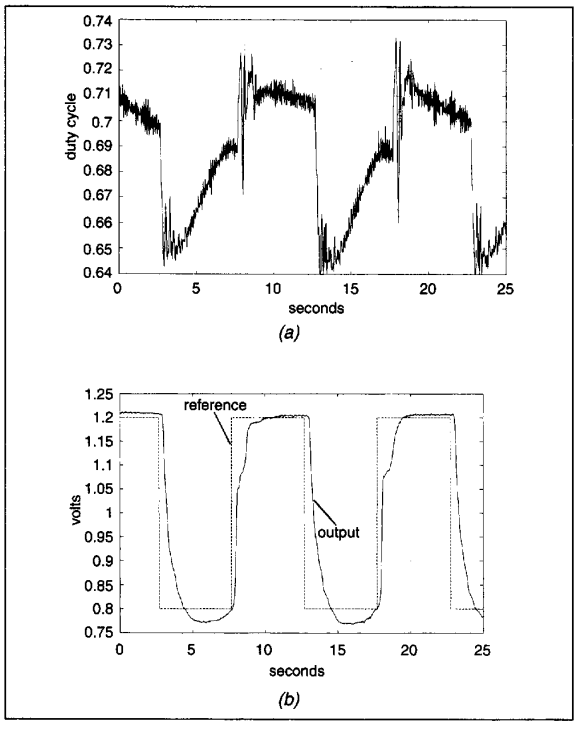

Fig. 7. High-order controller response: (a) duty cycle (b) output.

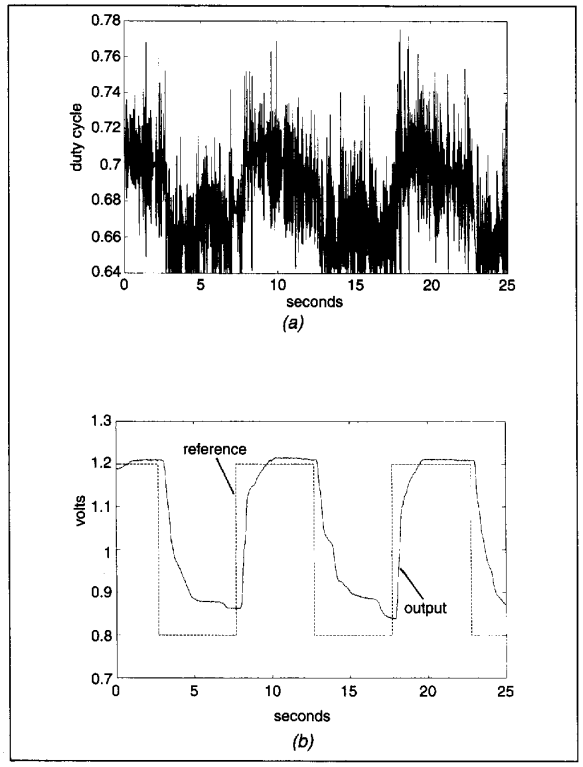

Fig. 8. Minimum-order controller response: (a) duty cycle (b) output.

tion, where muscle compactness, control and power/weight output are of paramount importance.

The adaptive control scheme has significantly improved the performance of the closed-loop system. Accuracies of 1° (0.045 volts) are easily achieved at the elbow joint for constant set-points. The closed-loop bandwidth is, however, low. Further work is needed to speed up the system response by selecting different polynomials in (16). Selection of sampling rates, operating pressures, and period of the pulse width modulator will also be addressed.

References

[1] P.J. McKerrow, "Introduction to Robotics," Addison-Wesley, 1991.

[2] D.G. Caldwell, "Compliant Polymeric Actuators as Robot Drive Units," Ph.d thesis, University of Hull, 1989.

[3] ——, "Miniature and Micro Robotic Machines: Technology, Design, and Applications," Workshop S4, IEEE Rob & Auto., Atlanta, USA, 1993.

[4] P. Dario, C.Montesi, R.Valleggi, and M. Beramasco, "Endoscopic Manipulator with SMA-Actuated Tip and Grippers," ICAM, pp.300-06, Tokyo, Japan, Aug. 1993.

[5] Dynalloy, "Biometal Guide Book," Dynalloy Inc., Irvine, Cal., USA, 1989.

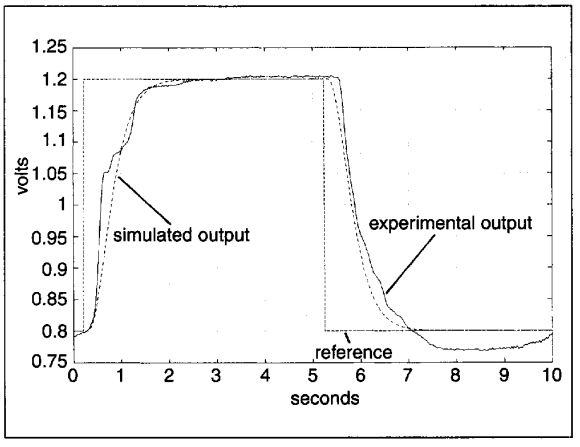

Fig. 9. Experimental response vs. simulation results.

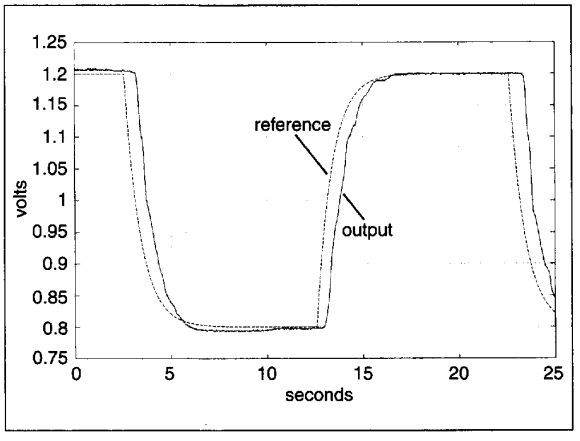

Fig. 10. Response for a smoothed square wave reference input.

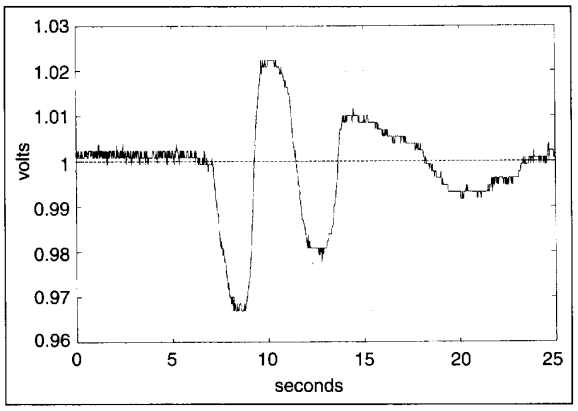

Fig. 11. Effects of supply pressure fluctuations.

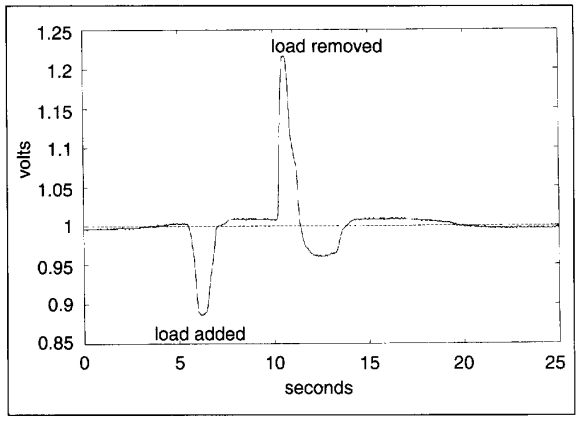

Fig. 12. Effects of load variations: (a) 0.15 Hz (b) 0.31 Hz (c) 0.62 Hz.

[6] D. Scott, "Electro-Rheological (ER) Fluid Near Commercial Stage," *Automotive Eng.*, vol. 93, pp. 75-9, Nov. 1985.

[7] H. Block and J.P. Kelley, "Electro-Rheology," *Journal of Physics D: Applied Physics*, vol.21, 1988, pp. 1661-77.

[8] A. Katchalsky, "Rapid Swelling and Deswelling of Reversible Gels of Polymeric Acids by Ionization," *Experimentia*, vol. 5, pp. 319-320, 1949.

[9] D.G. Caldwell and P.M. Taylor, "Chemically Stimulated Pseudo-Muscular Actuation," *Int. J. Of Eng. Science*, pp. 797-808, vol. 28, no. 8, 1990.

[10] D.G. Caldwell, "Natural and Artificial Muscle Elements as Robot Actuators," *Mechatronics*, vol. 3, no.3, pp. 269-283, 1993.

[11] A. Wassermann,"Size and Shape Changes of Contractile Polymers," ed. Pergamon Press, London, 1960.

[12] A. Waters, "The Magneto-Elastic Effect," Williams Press, York, 1990.

[13] R.W. Henke, "Introduction to Fluid Power Circuits and Systems," Addison-Wesley, 1969.

[14] F.Q. Hu, J.M. Watson, P.A. Payne, and M. Page, "A Fast Opto-Pneumatic Converter for Pneumatic Actuation," *IEE Colloquium on Robot Actuators, Digest 1991/146*, pp. 101-2, 1991.

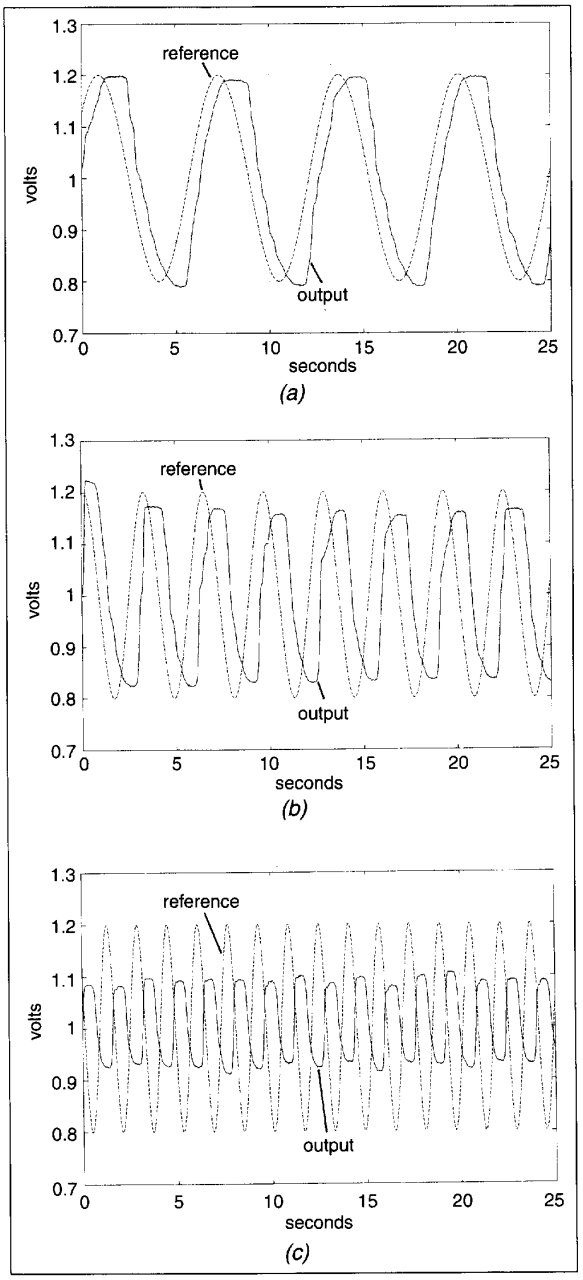

Fig. 13. Response to sinusoidal reference waveforms: (a) 0.15Hz (b) 0.31Hz (c) 0.62Hz.

[15] R.A.Schulte, "The Characteristics of the McKibben Artificial Muscle." In *The Application of External Power in Prosthetics and Orthetics*, publ. 874, Nas-RC, pp. 94-115, 1962.

[16] J.M. Winters, "Braided Artificial Muscles: Mechanical Properties and Future Uses in Prosthetics/Orthetics," RESNA 13th Conf., Washington, USA, pp. 173-174, 1990.

[17] K.Inoue, "Rubbertuators and Applications for Robots," *Robotics Research: 4th International Symposium*, and R. Bolles and B. Roth, eds. MIT Press, 1988.

[18] S.D. Prior and P.R. Warner, "Wheelchair Mounted Robots for the Home Environment," *IROS'94*, Yokohama, Japan, pp. 1194-2000, July 1993.

[19] D.G. Caldwell, A. Razak, and M.J. Goodwin, "Braided Pneumatic Muscle Actuators," IFAC Conf. on Int. Autonomous Vehicles, Southampton, UK, April 1993.

[20].Bridgestone Corp., "The Rubbertuator," product literature, 1988.

[21].C.P. Chou and B. Hannaford, "Static and Dynamic Characteristics of McKibben Pneumatic Artificial Muscles," IEEE Conf on Robotics and Automation, San Diego, USA, May, 1994.

[22] S.C. Jacobsen, E.K. Iversen, D.F. Knutti, et al., "Design of the Utah/MIT Hand," IEEE Conf. on Rob. and Auto., San Francisco, 1986.

[23] V. Kumar, T.G. Sugar, and G.H. Pfreudschuh, "A 3-Degree-of-Freedom in Parallel Actuated Manipulator," *9th CISM-IFToMM Sym. on Theory & Practice of Robots and Manipulator*, pp. 57-8, Udine, Italy, 1992.

[24] D.G.Caldwell, G.A. Medrano-Cerda, and M. Goodwin, "Braided Pneumatic Muscle Actuator Control of a Multi-jointed Manipulator," *IEEE SMC Conf.*, vol.1., pp. 423-38, Le Touquet, France, 1993.

[25] M.M. Mustafa and G.A. Medrano-Cerda, "On the Use of High Order Controllers to Improve the Robustness and Performance of Pole-Assignment Controllers," *28th IEEE Conf. Decision and Control*, Tampa, Florida, USA, pp. 1234-35, 1989.

[26] M.M. Mustafa, "Pole-Assignment High Order Controllers and Applications to Adaptive Control with On-Line Supervision," Ph.D. thesis, Dept. of Elec. Eng., Uni. of Salford, 1989.

[27] E.E. Eldukhri, "Adaptive Position Control of a DC Motor Based on a Robust Controller Design," M.Sc. thesis, Dept. of Elec. Eng., Univ. of Salford, 1991.

Darwin G. Caldwell received his B.Sc. in electronic control and robot engineering from the University of Hull in 1986 and his Ph.D. in robotics in 1990. Since 1990 he has been a lecturer in the Department of Electronic and Electrical Engineering at the University of Salford. His current research interests include actuators design, tele-presence robotics, dexterous manipulations, and tactile sensing and sensory feedback.

G.A. Medrano-Cerda received the B.Sc. degree of in electrical engineering from the Universidad Nacional Autonoma de Mexico in 1977, and the M.Sc. and Ph.D. degrees in control systems from Imperial College, London, in 1979 and 1982, respectively. From 1982 to 1985 he was an associate professor at the Division de Estudios de Postgrado, Facultad de Ingenieria, Universidad Nacional Autonoma de Mexico. From 1985 to 1986 he was a research fellow at the Department of Engineering, University of Warwick. Since 1986 he has been with the Department of Electronic and Electrical Engineering at the University of Salford. His current research interests are in the areas of robust control, adaptive control, neural networks, and advanced robotic applications.

Mike Goodwin received his B.Sc. degree in electronic and electrical engineering from the University of Salford in 1991. From 1992 to 1993 he was a research assistant in the Department of Electronic and Electrical Engineering at Salford University. From 1993-94 he worked as a research assistant at the ARTS lab Scuola Superiore S. Anna, Pisa, designing a high-level control system for an advanced mobile robot. Currently Mike works for British Rail as a signals and telecommunications engineering trainee and is completing his Ph.D.